In situ ellipsometry monitoring of TiO 2 atomic layer deposition from Tetrakis(dimethylamido)titanium(IV) and H 2 O precursors on Si and In 0.53 Ga 0.47 As substrates

E.V. Skopin, K. Abdukayumov, P. Abi Younes, M. Anikin, H. Roussel, J.-L. Deschanvres, H. Renevier

In situ ellipsometry monitoring of TiO_2 Atomic Layer Deposition from TDMAT and H_2O precursors on Si and $In_{0.47}Ga_{0.53}As$ substrates

E.V. Skopin[a,b,**], K. Abdukayumov[a], P. Abi Younes[a], M. Anikin[a], H. Roussel[a], J.-L. Deschanvres[a], H. Renevier[a,**]

[a] *Univ. Grenoble Alpes, CNRS, Grenoble INP*, LMGP, 38000 Grenoble, France. * Institute of Engineering Univ. Grenoble Alpes*

[b] *Laboratoire des Technologies de la Microélectronique (LTM), UMR CNRS 5129, 17 Avenue des Martyrs, 38054 Grenoble Cedex 9, France*

Abstract

TiO_2 Atomic Layer Deposition (ALD) is used in microelectronics due to its ability to produce conformal thin films whose thickness is controlled at the sub-nanometer scale. Tetrakis(dimethylamido)titanium(IV) (TDMAT) and water are frequently used precursors for TiO_2 ALD, although there are still some differences in growth behavior in the literature. In this parametrical study, the growth of TiO_2 was controlled *in situ* by Spectroscopic Ellipsometry (SE) in combination with *ex situ* thickness measurements by X-Ray Reflectometry (XRR). The injection and purge times were optimized to reach self-saturation on the surface. We put in evidence two regions of the Growth Per Cycle (GPC) as a function of substrate temperature: GPC decreases from 0.8Å.cy^{-1} to 0.5Å.cy^{-1} as the temperature rises from 50 °C to 200 °C, and then GPC increases from 0.6Å.cy^{-1} to 0.9Å.cy^{-1} as the temperature rises from 250 °C to 350 °C. There is

*Fully documented templates are available in the elsarticle package on CTAN.

*E.V. Skopin

**H. Renevier

Email addresses: evgeniy.v.skopin@gmail.com, evgenii.skopin@cea.fr (E.V. Skopin), hubert.renevier@grenoble-inp.fr (H. Renevier)

URL: https://orcid.org/0000-0003-3751-9298 (E.V. Skopin), https://orcid.org/0000-0002-7020-6544 (K. Abdukayumov), https://orcid.org/0000-0002-3228-1121 (P. Abi Younes), (M. Anikin), https://orcid.org/0000-0001-6110-5760 (H. Roussel), https://orcid.org/0000-0003-4668-8501 (J.-L. Deschanvres), https://orcid.org/0000-0002-2317-9344 (H. Renevier)

no evidence of an *ALD window*. The stoichiometry of the layer grown at 200 °C, determined by X-ray Photoelectron Spectroscopy (XPS), is TiO_2 (1 Ti atom per 2 O atoms). The 200 °C as-grown sample becomes crystalline (Anatase crystals) after annealing 3 hours in air at 400 °C, or at 600 °C. The initial growth stages of TiO_2 were studied by SE and Atomic Force Microscopy (AFM). Regarding TiO_2 ALD on (100)Si substrate (with a native SiO_2), we observed a substrate enhanced growth which turned into steady-state ALD beyond 20-30 cycles. Additionally, TiO_2 ALD on (001)$In_{0.53}Ga_{0.47}As$ substrate demonstrates substrate inhibited growth of type 2 (islands formation) which turned into TiO_2 steady-state ALD beyond 20-30 cycles. The results of TiO_2 ALD are compared with those of the existing literature.

Keywords: Atomic Layer Deposition; Spectroscopic Ellipsometry; TiO_2; Oxides; TDMAT; Initial growth; Substrate Enhanced Growth; Substrate Inhibited Growth; InGaAs

---

1. Introduction

Titanium dioxide (TiO_2) or titania is a widely used material in microelectronics. The two polymorphs of titania - Anatase, and Rutile give TiO_2 its photocatalytic properties [1]. Titania is a transparent material in the near-infrared range. It has a high dielectric constant, a high refractive index. Thus, it finds a lot of applications in optics, catalysis, and electronics [2]. TiO_2 nanomaterials, nanoparticles, thin films, and nanowires are synthesized by various chemical and physical methods [2] such as Sol-Gel Method [3], Chemical Vapor Deposition [4, 5], Magnetron-Sputtering [6], and others [7].

One of the best-used technics for TiO_2 thin film deposition and nanostructure coatings is Thermal Atomic Layer Deposition (ALD) which provides a low temperature (50-200 °C) TiO_2 growth with high conformality and precise subnanometer thickness control [8]. Thermal ALD [9] is a Chemical Vapor Deposition (CVD) technique based on the self-limiting chemical reactions. The ALD process consists of ALD cycles. One cycle includes injections of precursors

(chemical compounds) that react with a temperature-controlled sample surface. In the case of TiO_2 ALD [10], a metal-organic Ti precursor and oxygen precursor are injected in the reactor chamber one after another. In between the precursor injections, the reactor chamber is purged with inert gas to remove reaction products and the remaining parts of the precursor.

The $TiCl_4$ (halide) precursor, one of commonly used Ti precursors, was used in early TiO_2 growth experiments [11]. However, a disadvantage of halides is the corrosiveness of the reaction byproducts. For instance, HCl is a reaction product of $TiCl_4$ with sample surface OH-group. Now, a lot of new Ti metalorganic precursors besides halides have been synthesized and used for ALD [10]: alkoxides, alkylamides, and heteroleptics. As oxidants [10], one can use H_2O, H_2O_2, O_2, O_3, MeOH, HCOOH, CH_3COOH, and some plasma sources (in case of Plasma Enhanced Atomic Layer Deposition – PEALD).

In this study, we consider the Atomic Layer Deposition using one of the most popular couples of precursors, *i.e.* $Ti[(CH_3)_2N]_4$ or Tetrakis(dimethylamido)titanium(IV) (hereinafter TDMAT) and water. Despite the significant number of publication reporting on TiO_2 ALD from TDMAT and water [12, 13, 14, 15, 16, 17, 18, 19, 20, 21, 22, 23, 24, 25, 26, 27, 28, 29, 30, 31, 32, 31, 33], there is no clear idea of all the possible chemical reactions on the surface during the growth process and also there is no unique behavior of growth curves (Growth Per Cycle) as a function of the growth temperature. Additionally, it was shown that the TiO_2 initial growth stages depend on substrate chemistry, as in the case of ZnO ALD [34, 35, 36, 37], TiO_2 exhibit different types of growth depending on the surface [15, 29].

In this article, we report on an extensive parametrical study of TiO_2 ALD from TDMAT and water, by monitoring the growth *in situ* with spectroscopic ellipsometry. Our results are compared with those obtained by other groups to find an explanation of some differences in GPC temperature and initial growth stage behavior.

2. Experiment

TiO_2 Atomic Layer Deposition (ALD) was carried out with TDMAT as the Ti metalorganic precursor, water as an oxidant, and N_2 as a purging gas. TDMAT bubbler and water evaporator were kept at room temperature (25 $°C$) during the experiment. During the first ALD cycle pulse, TDMAT was injected into a closed reactor chamber carried by a 50 *sccm* flow of Ar gas that was flowing into the TDMAT bubbler. Then, during the second pulse, the reactor chamber was purged with a 1000 *sccm* flow of N_2 to remove excess TDMAT, Ar, and the products of the TDMAT reaction. During the third pulse, water steam was injected inside the reactor chamber (closed), using a deionized water evaporator without carrier gas. Finally, during the fourth pulse, the reactor chamber was purged out with a 1000 *sccm* flow of N_2.

Silicon with a native SiO_2 layer on the top (from Sil'tronix) and $In_{0.53}Ga_{0.47}As(270\ nm)/InP$ (hereinafter InGaAs) substrates (from III-V lab, Palaiseau) were used for the experiment. SiO_2/Si substrates were not chemically treated before the growth. InGaAs substrates were etched in 4M HCl solution for 3 *min*, rinsed in deionized water for 30s, and dried with N_2 to remove native surface oxides. Then, InGaAs substrates were immediately annealed in a vacuum inside the growth chamber at 200 $°C$ for 30 *min* to remove atomic As on the surface [38, 34].

The growth was monitored *in situ* by spectroscopic ellipsometry. We used the 4 wavelengths (465 *nm*, 525 *nm*, 580 *nm*, and 635 *nm*) Film Sense FS-1^{TM} Banded Wavelength Ellipsometer and FS-1 software for thickness calculation [39]. The final TiO_2 thickness was measured by X-Ray Reflectometry (XRR) using a SIEMENS D5000 (Bruker^{TM}) reflectometer at the Cu K_α wavelength and Bruker Leptos (version 6.03) software for the data analysis. The substrate and TiO_2 layer surface morphology was studied by an Atomic Force Microscopy (AFM) using a Dimension Icon Bruker^{TM} microscope. The crystallographic transition was studied by Grazing Incidence X-Ray Diffraction (GIXRD) with a SmartLab (Rigaku^{TM}) and Fourier-Transform Infrared Spectroscopy (FTIR) with VERTEX 70v FT-IR Spectrometer. During GIXRD measurements, the

incident angle between the x-ray beam and the sample surface was 0.35° (above the critical angle $\alpha_c = 0.25°$ for Cu K_α). The elemental composition of TiO_2 was determined using X-ray Photoelectron Spectroscopy (XPS). XPS analyses were carried out in the K-alpha apparatus from Thermo Fisher Scientific. In an Ultra-High Vacuum (UHV) chamber (10-9 *mbar*), sample surfaces were irradiated with Al K_α radiation (1486.6 eV). The ejected electrons were collected by a hemispherical analyzer at 30 eV constant pass energy. The energy scale was calibrated with the C1s line from the contamination carbon at 285.0 eV. The measurements were carried out at a constant angle of 90° between the sample surface and the analyzer.

3. Results

3.1. TiO_2 Atomic Layer Deposition parametric study

To build the ellipsometry model for the calculation of the TiO_2 film thicknesses, the refractive index n as a function of wavelength λ was determined by the Cauchy equation:

$$n(\lambda[nm]) = n_{633nm} + n_{slope}((1000/\lambda)^2 - (1000/633)^2), \quad (1)$$

where the constants $n_{633nm} = 1.7$ and $n_{slope} = 0.069$ were determined on the grown TiO_2 sample with a known thickness, using the FS-1 software. The final TiO_2 thickness was also checked by XRR measurements (see Fig. 1S and Table T1 in the Supplementary Information file). More information about ellipsometry measurements with the same equipment and software can be found in a previous study [35].

Here, we report on a parametrical study to optimize TiO_2 ALD in our custom-built reactor [40, 34, 36, 35, 41, 37]. The main process parameters were varied, *i.e.* the duration of TDMAT injection ($t_{TDMAT\ inj.}$), TDMAT purge ($t_{TDMAT\ purge}$), water injection ($t_{H2O\ inj.}$), and water purge ($t_{H2O\ purge}$), the water flow during water injection, as well as the substrate temperature. Also, we checked the influence of the substrate surface of growth on the early stage of

growth ((100)Si and (100)InGaAs/InP). The parametric study was performed on Si substrates.

First, we carried out TiO_2 ALD on Si for a series of samples by changing $t_{TDMAT\ inj.}$: 2s, 5s, 7s, 10s, 20s, 30s, and 60s. The other injection/purge times $t_{TDMAT\ purge}/t_{H2O\ inj.}/t_{H2O\ purge}$ were fixed to 30s/30s/45s, respectively; the water flow was 7.5 *sccm*; and the substrate temperature was 150 $°C$ (this substrate temperature was often used for TiO_2 ALD using TDMAT and water [12, 14, 19, 21, 42, 25, 30, 32], it is lower than TDMAT decomposition temperature [43], and high enough to avoid water condensation on the substrate surface [44, 42]).

Figure 1 shows the film thickness, measured *in situ* by ellipsometry, as a function of the number of cycles for different $t_{TDMAT\ inj.}$ (injection time). The inset shows a zoom of one curve ($t_{TDMAT\ inj.} = 60s$) corresponding to the cycle range 37 to 40. One can see that during TDMAT injection, the thickness starts to increase, then reaches a constant value. In contrast, during water pulse, the thickness decreases due to ligand exchange and OH-groups formation on the surface, then thickness reaches a constant value.

Comparing the thickness curves on Fig. 1, one can see that the steady growth rate increases for higher TDMAT injection times, till it reaches a maximum value. Note that all the curves show a non-linear dependence as a function of cycle number, *i.e.* the first derivative of the mean thickness starts to decrease then becomes constant (steady growth). To determine the right TDMAT injection time value, we plotted the Growth Per Cycle (GPC) as a function of TDMAT injection time. First, we calculated GPC as a function of cycle number as shown in the inset of Fig. 1: the GPC for cycle n is the variation in thickness observed between cycles n and (n-1), the thickness value is measured in the water purge region. Then, using this GPC function, we calculated the mean GPC value in the steady growth state region (for instance, for the curve corresponding to $t_{TDMAT\ inj.} = 2s$, this region is within the range of 30 to 50 cycles). Figure 2(a) shows the mean GPC corresponding to the steady growth as a function of TDMAT injection time. The plot shows that increasing the

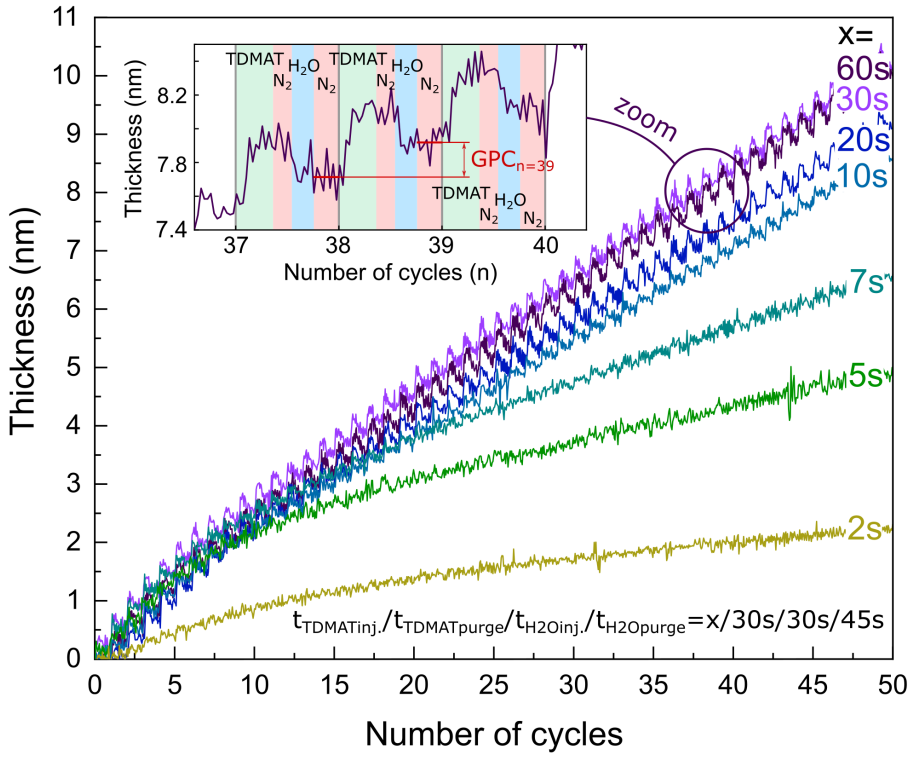

Figure 1: TiO_2 thickness as a function of cycle number measured for different TDMAT injection time during growth (2s, 5s, 7s, 10s, 20s, 30s, and 60s). Inset: zoom of the 60s curve in the cycle range 37 to 40.

TDMAT injection time from 0 to 10s, the GPC linearly increases from 0 to 1.6Å.cy^{-1}. Then, the rate of GPC increase becomes smaller for injection times within the range of 10s to 30s. At about 30s injection time, the GPC reaches a plateau at a constant value close to 1.9Å.cy^{-1}. Since TDMAT injection time has to be low enough to save experimental time and prevent the waste of precursor, but high enough to reach self-limiting surface saturation (GPC plateau), it was fixed to 10s (green open circle on Fig.2(a)).

After optimizing the TDMAT injection time, we optimized the TDMAT purge time ($t_{TDMATpurge}$). The pulse times $t_{TDMAT\ inj.}/t_{TDMAT\ purge}/t_{H2O\ inj.}/t_{H2O\ purge}$ were fixed to 10s/x/30s/45s, respectively, where $x = t_{TDMATpurge}$ was fixed to 5s, 30s, 60s, and 180s. Fig.2(b) shows GPC as a function of TDMAT purge

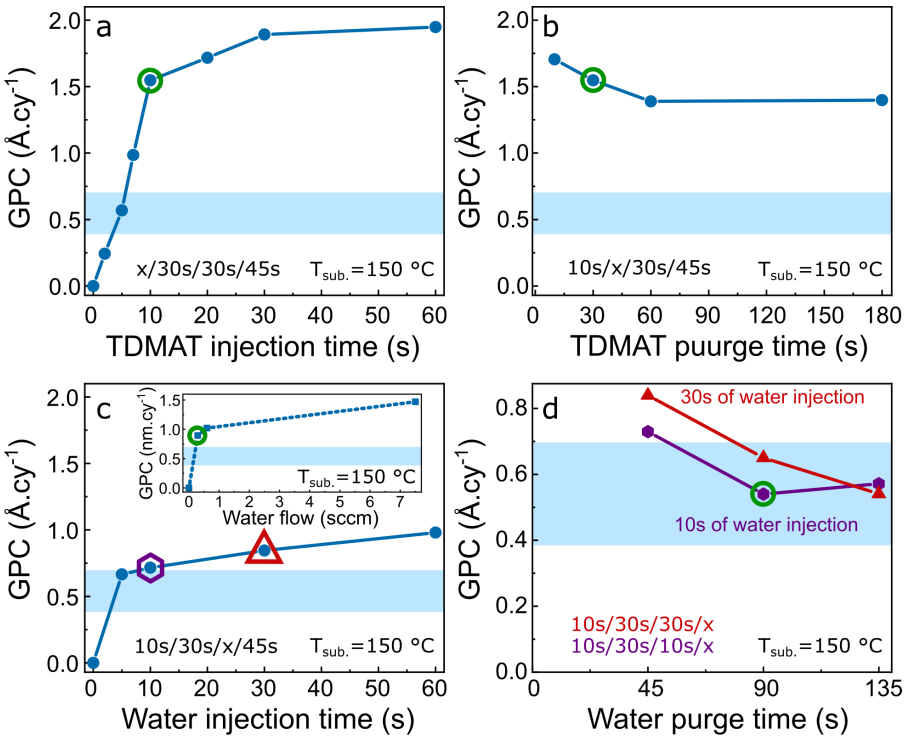

Figure 2: Growth Per Cycle (GPC) as a function of TDMAT injection time (a), TDMAT purge time (b), water injection time (c), water flow (c, inset), and water purge time (d). The green open circles on the figure show our optimized growth parameters. Violet solid hexagons and red solid triangles on panel (d) show the GPC behavior for 10s and 30s water injection times, respectively. The light blue area in the background indicates the range of expected TiO_2 GPC values as found in the literature [12, 14, 19, 21, 42, 25, 30, 32].

time. Increasing TDMAT purge time from 5s to 180s, the GPC decreases from 1.6Å.cy^{-1} to 1.4Å.cy^{-1}. We decided to fix the TDMAT purge time to 30s (green open circle on Fig.2(b)).

Although TDMAT injection and purge times were optimized, the total GPC for this substrate temperature (150 $°C$) is higher than GPC found in the literature [12, 14, 19, 21, 42, 25, 30, 32] (light blue region on figure.2(a)-2(d)). Thus, we checked the influence of water injection and purge times on the process. Since the reactor chamber was closed during water pulse, an increase of water flow and/or water injection time results in an increase of water amount inside

the reactor chamber. Figure 2(c) shows steady GPC values as a function of water injection time, $t_{H2O\ inj.}$ with $t_{TDMAT\ inj.}/t_{TDMAT\ purge}/t_{H2O\ purge}$ fixed to 10s/30s/45s; and water flow fixed to 0.3 *sccm*. The inset of Fig. 2(c) shows the GPC as a function of water flow values. Both GPC curves increase for higher water injection time or flow, then reach a constant value. The optimized water flow was fixed to 0.3 *sccm* (green open circle), and the water injection time to 10s (violet open hexagon) or 30s (red open triangle).

Figure 2(d) shows two GPC curves obtained upon water purge time, for 10s of water injection (violet solid hexagones) and 30s of water injection (red solid triangles), $t_{TDMAT\ inj.}/t_{TDMAT\ purge}$ were fixed to 10s/30s. Both curves reach the same value equal to 0.55Å.cy^{-1} for 135s water purge time, and for both curves, the GPC decreases when the water purge time increases. However, in comparison to 30s of water injection, lower water purge times are needed to reach the GPC plateau for 10s of water injection.

Based on this, we chose the following process parameters: $t_{TDMAT\ inj.}/t_{TDMAT\ purge}/t_{H2O\ inj.}/t_{H2O\ purge}$ equal to 10s/30s/10s/90s, respectively and the water flow equal to 0.3 *sccm*, to determine the GPC versus the substrate temperature. Figure 3 shows the experimental GPC values as a function of substrate temperature determined in this study (blue solid circles), as well as values from the literature [12, 14, 19, 21, 42, 25, 30, 32] obtained for ALD TiO_2 layers grown from TDMAT and water.

It clearly appears that the GPC behavior as a function of the growth temperature can be divided into two regions: the GPC decreases from 0.8Å.cy^{-1} to 0.5Å.cy^{-1} as the temperature rises from 50 $°C$ to 200 $°C$, then it increases from 0.6Å.cy^{-1} to 0.9Å.cy^{-1} as the temperature rises from 250 $°C$ to 350 $°C$. The origin of this behavior is discussed hereafter in the Discussion section (section 4).

3.2. Stoichiometry of TiO_2 amorphous layers and TiO_2 crystallization after annealing

To check the stoichiometry of the ALD TiO_2 layers and chemical states of Ti and O atoms, we performed X-ray Photoelectron Spectroscopy (XPS) measure-

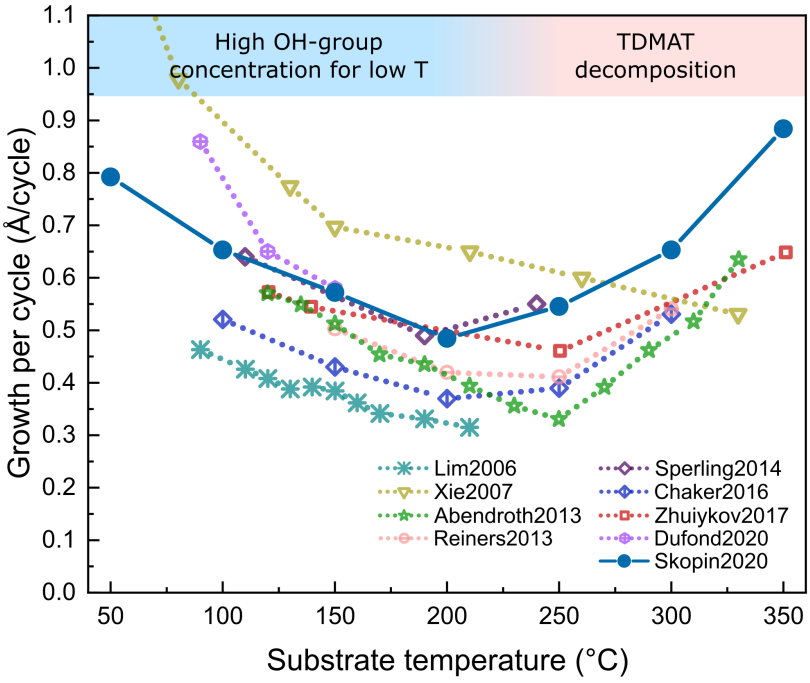

Figure 3: Experimental Growths Per Cycle (GPCs) as function of substrate temperature: present study (blue solid circles, solid line), and from the literature [12, 14, 19, 21, 42, 25, 30, 32](different types of open symbols, dashed lines).

ments. Here, we give the results for a sample obtained with the following growth conditions: 200 $°C$, 275 cycles, deposition times equal to 10s/30s/10s/45s (see Fig.2(d)). The water flow during deposition was set to 0.3 $sccm$. The XPS signal was measured from the as-grown TiO_2 subsurface, and then the measurement was repeated after 3 min of a surface etching by Ar plasma (approximately 3-4 nm thick TiO_2 layer was etched). Figure 4(a) shows Ti2p XPS lines measured before Ar etching, other XPS lines before and after etching are presented in the Supplementary Information (figure S2). The Ti2p spectra consists of $Ti2p_{3/2}$ and $Ti2p_{1/2}$ peaks (doublet). The peak positions correspond to the ones of stoichiometric TiO_2 [32, 45, 46]. Other elements were also found in the layer: O, N, and C. Integrating the area for every element and using the relative sensitivity factors (RSF) method, we calculated the atomic percent of every element in the

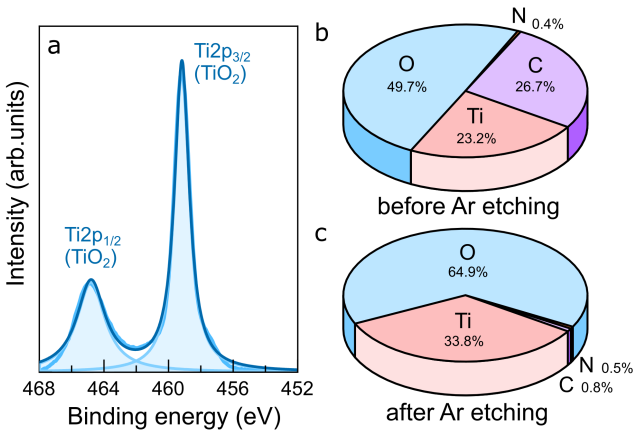

Figure 4: X-ray Photoelectron Spectroscopy (XPS) of Ti 2p lines (doublet): intensity as a function of binding energy measured before Ar plasma etching (a); element concentrations in TiO_2 layer in atomic percent measured before (b) and after (c) Ar plasma etching.

film. Figure 4(b) shows the atomic percent of the film surface and subsurface before plasma etching, *i.e.* 23.2%, 49.7%, 0.4%, and 27.7% of Ti, O, N, and C; respectively. After Ar plasma etching (figure 4(c)), the C content almost drops down to zero, and the relative concentration of Ti, O, and N stays the same, *i.e.* 33.8%, 64.9%, 0.5%, 0.8% of Ti, O, N, and C, respectively. Thus, before and after plasma etching, the TiO_2 stoichiometry is approximately one Ti atom for every two O atoms.

Grazing Incidence X-Ray Diffraction (GIXRD) and Fourier-Transform Infrared Spectroscopy (FTIR) measurements showed that the sample grew at 200 $^{\circ}C$ is non-crystalline. For improving the crystallinity of the as-deposited TiO_2 layer we annealed a set of samples deposited at 200 $^{\circ}C$ on Si substrate (same growth conditions as mentioned in the first paragraph of this section) in the air for 3h at 400 $^{\circ}C$ and 600 $^{\circ}C$.

Figure 5(a) shows GIXRD diagrams measured for the as-deposited and annealed TiO_2/Si samples. After annealing one can observe the Bragg peaks of TiO_2 Anatase structure (ICSD 9852, PDF 01-071-1166), regardless of the annealing temperature. On all diagrams one can see a bump located around 50-60°, we suppose that it is caused by the diffuse scattering from the Si substrate.

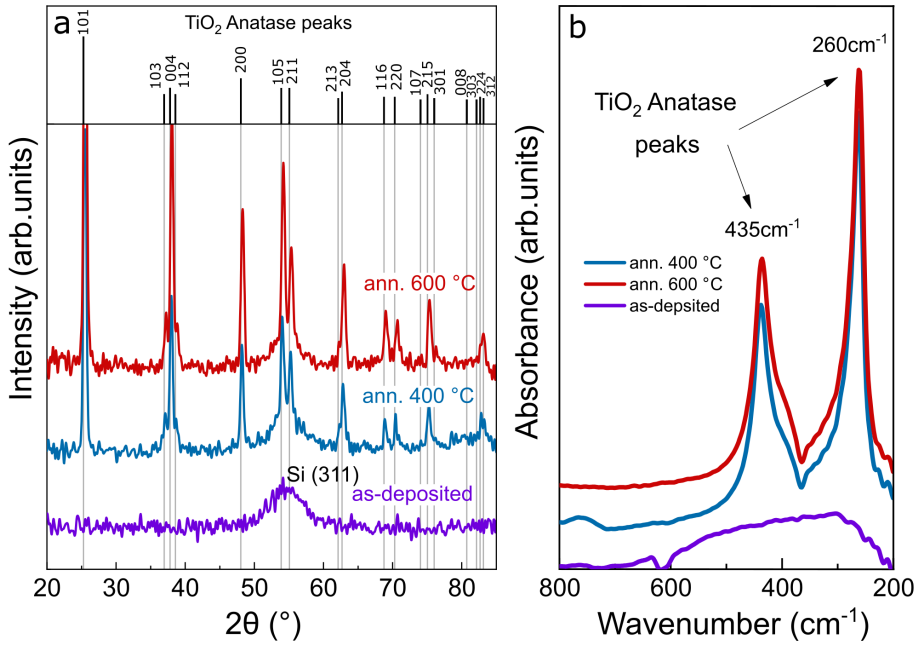

Figure 5: Grazing Incidence X-Ray Diffraction (GIXRD) (a) and Fourier-transform infrared spectroscopy (FTIR) (b) curves measured for the as-deposited sample (deposition temperature was 200 °C) and for samples annealed at 400 °C and 600 °C.

FTIR measurements (figure 5(b)) confirm the same result with the presence of the two characteristic peaks of TiO_2 Anatase [47] at 435 cm^{-1} and 260 cm^{-1}.

3.3. TiO_2 initial growth on Si and $In_{0.53}Ga_{0.47}As$

In this section, we report on a study of the early growth of ALD TiO_2 on (100)InGaAs and (100)Si substrates. The latter being covered with native silicon oxide. The deposition temperature was 150 °C and the $t_{TDMAT\ inj.}/t_{TDMAT\ purge}/t_{H2O\ inj.}/t_{H2O\ purge}$ were 10s/30s/30s/45s, respectively, the water flow was 0.3 *sccm*. We grew a series of samples with 2, 5, 10, and 15 cycles. The InGaAs substrate surface presents atomically flat terraces, therefore the surface morphology change could be easily detected by Atomic Force Microscopy (AFM). Figure S3 in Supplementary Information shows AFM images for ALD TiO_2 on InGaAs and Si.

Figures 6(a) and 6(b) show the *in situ* GPC versus cycle number for ALD TiO_2 grown on InGaAs and Si, respectively. The insets of Figs. 6(a) TiO_2/InGaAs

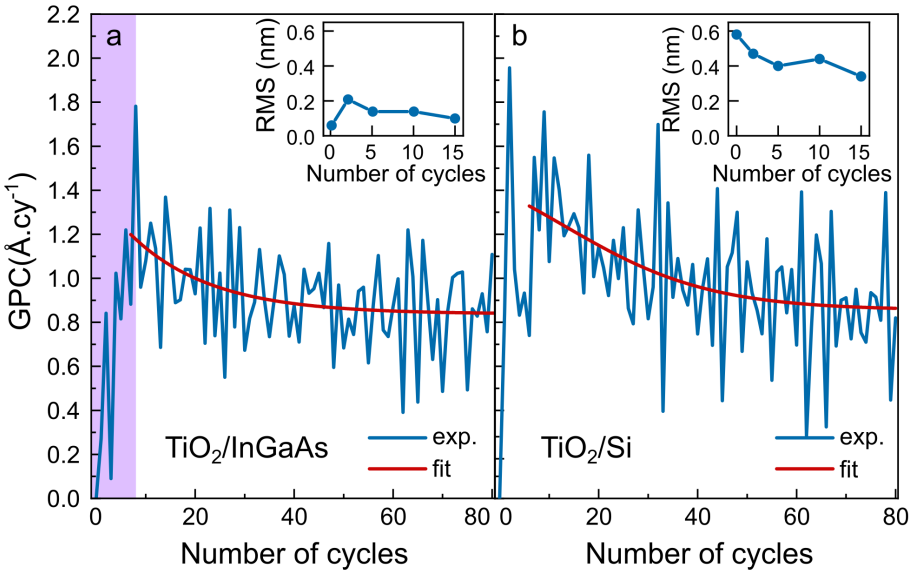

Figure 6: GPC versus cycle number measured during TiO_2 ALD on InGaAs (a) and Si (b). The light violet area on the left panel (a), highlight the region where the GPC increases. The figure insets show the surface roughness (root mean squared roughness).

and 6(b) TiO_2/Si show TiO_2 surface Root Mean Squared (RMS) roughness, calculated using a series of AFM images (image size was $(1x1)\mu m^2$), as a function of the number of cycles.

Each GPC curve for TiO_2/InGaAs and TiO_2/Si has transient growth region prior to linear growth (constant GPC). One can observe that the GPC of TiO_2 ALD on InGaAs can be divided into three regions, at the early stage it increases up to a maximum (light violet area), then slightly decreases before reaching a constant value. In comparison, in the case of TiO_2/Si, the growth region corresponding to the increase of GPC is absent. Beyond cycle 2, both GPC curves demonstrate the same behavior. The red lines on the GPC curves represent the Sigmoid function fits, plotted for better data visualization.

At the same time, beyond 2 ALD cycles the RMS roughness of ALD TiO_2/InGaAs increases whereas it decreases for ALD TiO_2/Si. Then, increasing the number of cycles, TiO_2 roughness starts to decrease both for TiO_2/InGaAs and TiO_2/Si.

4. Discussion

In an attempt to explain our results about the growth of TiO_2 by ALD, we need to describe the possible chemical reactions on the growth surface. In the present study, one cycle of thermal TiO_2 ALD from TDMAT and water consists of four pulses: TDMAT injection, TDMAT purge (N_2), water injection, and water purge (N_2). As shown by experiments, Density Functional Theory (DFT) and Monte-Carlo (MC) simulations [14, 42, 12, 19, 30], TDMAT interaction with OH-terminated surface can be formally described by the following chemical reaction:

$$-OH^* + TiL_4 \rightarrow -O - TiL_3^* + HL, \tag{2}$$

where -OH^* is a hydroxyl group on the TiO_2 surface (* denotes the surface species), TiL_4 is a TDMAT molecule, L (or $N(CH_3)_2$) a TDMAT ligand, and HL ($H(N(CH_3)_2)$) the dimethylamine (DMA). Then, TiL_3, chemisorbed on the surface, can react with another surface OH-group and lose one ligand L to form DMA:

$$-OH^* + -TiL_3^* \rightarrow -O - TiL_2^* + HL, \tag{3}$$

After reaction with TDMAT, TiO_2 surface becomes L-terminated, and the reaction products are eliminated. During water injection, H_2O reacts with L-terminated TiO_2 surface:

$$-TiL_n + H_2O \rightarrow -TiL_{(n-1)}OH + HL, \tag{4}$$

Finally, TiO_2 surface becomes OH-terminated, and the reaction products of the are purged. Then, a new ALD cycle can start.

4.1. Growth per cycle as a function of substrate temperature

Experiments and calculations show that the GPC depends on the chemical reactions between the selected precursors and the sample surface, which strongly depend on the surface temperature [8]. Dufond *et al.* [32], using Density Functional Theory (DFT) and Monte Carlo (MC) calculations, showed that the volume of the TDMAT molecule is rather large (220.4 $Å^3$) and that the

GPC falls in the range of [0.18-0.26] monolayer/cycle, depending on the substrate temperature. The GPC is lower than the Anatase lattice parameters a = 3.78520Å, c = 9.51390Å(ICSD 9852, PDF 01-071-1166), this can be explained by the TDMAT steric hindrance.

As shown in figure 3, the substrate temperature is a factor that strongly influences the GPC. To explain the GPC behavior and connect it with chemical reactions (2), (3) and (4) that happen on the surface, growth is considered in two temperature ranges (below or above than 200 $°C$).

First, let us consider reaction (2) in the low-temperature range (50-200 $°C$). Xie *et al.* [14] showed that TDMAT molecule can be easily chemisorbed on TiO_2 surface covered with OH-groups. This reaction can occur at all temperatures (from room temperature upwards).

Reaction 4 determines the number of OH-groups on the growth surface and has an impact on GPC. Walle *et al.* [44], using synchrotron radiation core level photoelectron spectroscopy (XPS), showed that concentration of OH-groups and water molecules on the TiO_2 surface decreases while increasing the surface temperature. Consequently, one can expect higher GPC at lower substrate temperatures due to an increase in the number of active surface sites (OH-groups, water molecules, protons) to react with TDMAT. Indeed, using *in situ* reflection-absorption infrared spectroscopy (RAIRS) during TiO_2 ALD from TDMAT and water precursors, Sperling *et al.* [42] showed that water molecules are present on the growth surface at 110 $°C$ and 190 $°C$. Instead, the authors showed that that at 240 $°C$, water molecules on the surface are not consumed by TDMAT, indicating that water has desorbed from the surface during the TDMAT pulse. In general, several studies [12, 14, 19, 21, 42, 25, 30, 32], including ours, demonstrate that the GPC decreases as the substrate temperature increases in the low-temperature range.

Now, for higher substrate temperatures ($T_{sub.} > 200°C$), the density of the OH-groups on TiO_2 surface is expected to decrease [44] resulting in a decrease in total CPC which can be offset by an increase due to the decomposition of the TDMAT precursor molecules. Driessen *et al.* [43] used infrared spectroscopy *in*

situ to study the TDMAT decomposition on the growth surface. They showed that for substrate temperatures higher than 200 $°C$, TDMAT decomposes and forms TiN_xC_y compounds on the surface. They showed that time is an important parameter in the TDMAT decomposition process. Given their experimental condition, it was necessary to wait several minutes to decompose all the TDMAT precursor amounts and increasing the substrate temperature the decomposition becomes faster. Sperling *et al.* [42] used XPS to check whether a higher carbon concentration is detected in the material grown at higher temperatures (240 $°C$) during the ALD process. They found that the C concentration during the real ALD process decreases as a function of substrate temperature (1.4, 0.7, 0.7 at.% at 110, 190, 240 $°C$, respectively).

Besides, Xie *et al.* [14], using DFT calculations, suggested that during ALD, the desorption of the intermediate product of the reaction, *i.e.* TiL_3-OH, is possible, although the energy barrier is quite high (1.39 eV). The authors experimentally demonstrated that this effect can contribute to the decreasing of the GPC at high temperatures (greater than 200 $°C$). Thus, both the TiL_3-OH desorption from the surface and the TDMAT decomposition on the surface influence the GPC values in the high-temperature range of growth. Figure 3 shows that the experimental GPC increases in the high-temperature range of growth as reported in almost all studies of TiO_2 ALD from TDMAT and water. Since the chemical reactions during TDMAT pulse are no longer self-limited at high temperatures, the GPC values depend on the amount of injected TDMAT. As a consequence, GPC values in the reported literature[19, 21, 42, 25, 30, 32] are not consistent.

4.2. The initial TiO_2 growth

The incipient TiO_2 ALD from TDMAT and water is different for (100)InGaAs or (100)Si (covered with native oxide) surfaces, but in both cases, a transient regime of growth precedes the steady-state one. As shown in figure 6(a), the early stage of TiO_2 ALD on (100)InGaAs is typical of a substrate-inhibited growth of type 2 [48] (GPC increases, reaches the maximum, then starts to

decrease before reaching a constant value corresponding to the steady-state of growth). Instead, TiO_2 ALD on Si (Fig. 6(b)) is typical of a substrate-enhanced growth [48] (GPC is maximum at the first cycle, then starts to decrease to reach a constant value).

Similarly to the previous case, Dendooven *et al.* [15], using *in situ* Ti X-Ray Fluorescence (XRF) monitoring during TiO_2 ALD from TDMAT and water, demonstrated a substrate-enhanced growth of TiO_2 on Al_2O_3 surface. They hypothesized that Al_2O_3 surface had a higher surface density of OH-groups than the TiO_2 surface. They also showed that TiO_2 GPC grown on HF-etched Si surface is low at the beginning of growth, then it rises and reveals a substrate-inhibited growth of type 2 [48]. The authors assigned the low GPC value during the first cycles to the lower OH-group concentration on the HF-treated Si surface than on TiO_2 surface.

Interestingly, Ye *et al.* [29], using *in situ* infrared spectroscopy during TiO_2 ALD on GaAs, demonstrated that chemical adsorption of TDMAT is higher to chemical oxide on GaAs surface (their substrates were treated for 30 *min* in an aqueous H_2O_2 solution to grow a chemical oxide layer, followed by a deionized water rinse and N_2 blow-dry) than to as-grown TiO_2 surface, possibly leading to substrate enhanced growth.

In our previous ALD study [34, 35, 36, 37], we showed that the early stage of growth of ZnO ALD on (100)InGaAs surface from Diethylzinc and water, is a substrate-inhibited growth of type 2, as in the case of TiO_2 ALD on (100)InGaAs. As for TiO_2 ALD on InGaAs, the most likely explanation for the GPC behavior in the early stage of growth, is the surface roughening (see inset of Fig. 6(b)). After the first cycle, the surface area available for the reaction increases due to the formation of nuclei or islands and leads to the increasing of the GPC [34]. Then, the surface becomes smooth (the surface area decreases), and GPC decreases to reach a constant value.

With respect to the case ZnO ALD on (100)InGaAs, the origin of higher TiO_2 GPC during the first cycles on Si (covered with a native Silicon oxide) is likely due to a higher density of OH-groups (or water molecules) on the native

Si oxide surface than on the grown material surface.

4.3. Crystallization of amorphous TiO_2 layers

Most studies on TiO_2 thermal ALD, using TDMAT and water as precursor and oxidant, show that TiO_2 thin films are amorphous (according to XRD) after deposition at temperatures less than 250 $^\circ C$ on (100)Si covered with native SiO_2 [19, 31, 12, 14], (100)Si without native oxide [32], SiO_2(430 nm)/Si [21], RuO_2/Ru electrodes grown on SiO_2/Si [25], and SiC fiber bundles [24].

Chaker *et al.* [25] showed that as-deposited 18 nm-thick TiO_2 layers, grown at 250 $^\circ C$ from TDMAT and water, is composed of TiO_2 Anatase with a small amount of TiO_2 Rutile crystalline phases. Abendroth *et al.* [19] showed that as-deposited 47 nm-thick TiO_2 layer, grown at 320 $^\circ C$ from TDMAT and water, both TiO_2 Anatase and Rutile phases are detected. The authors found that 10 nm-thick TiO_2 layer grown at 250 $^\circ C$, is amorphous, whereas, for higher thicknesses, the nucleation of crystalline phases is initiated inside the layer. For deposition temperatures higher than 250 $^\circ C$, nucleation of the crystalline layer can start directly on the (100)Si substrate (covered with a native SiO_2 layer). Reiners *et al.* [21] found different crystalline phases of TiO_2 deposited at different substrate temperatures (using TDMAT and water): up to 200 $^\circ C$ - no crystalline phases; at 250 $^\circ C$ - the brookite and Anatase phases; at 300 $^\circ C$ - the Brookite, Anatase, and Rutile phases.

Summarizing the experimental findings from the literature, one can say that, for substrate temperature equal to or greater than 250 $^\circ C$, the TiO_2 crystallization starts during the ALD process [32].

In the present study, we have shown that as-deposited, about 14 nm-thick TiO_2 layer, grown at 200 $^\circ C$ on (100)Si, is amorphous. And it becomes crystalline after 3 hours of annealing in air. Regardless of the temperature, 400 $^\circ C$ or 600 $^\circ C$, the crystalline phase is Anatase.

Several annealing experiments reported in previous studies are in agreement with our results. Lim *et al.* [12] showed that ALD TiO_2 layer deposited at 150 $^\circ C$ (from TDMAT and water) is amorphous. After annealing 3 hours in the

air it becomes crystalline and shows the presence of Anatase phase at annealing temperatures in the range [300-400 $°C$], both Anatase and Rutile phases in the range [500-700 $°C$], and only Rutile phase at 800 $°C$. Cao *et al.* [24] showed that 70 nm-thick ALD TiO_2 (from TDMAT and water) layer grown at 150 $°C$ is amorphous, it becomes crystalline after a thermal treatment. Annealing for one hour in the air at 600 $°C$ leads to Anatase; 1000 $°C$ to Anatase and Rutile; then 1400 $°C$ to Rutile. Xie *et al.* [14] showed that ALD TiO_2 deposited layers at 150 $°C$ (from TDMAT and water) are amorphous, they crystallize to Anatase after annealing in the temperature range [400-600 $°C$].

5. Conclusion

Using *in situ* Spectroscopic Ellipsometry (SE) and together with post-growth X-Ray Reflectometry (XRR), we monitored TiO_2 ALD on Si and InGaAs substrates. We found that the TiO_2 ALD from TDMAT and water precursors can be split into two temperature regions: a low-temperature range (50-200 °C) in which GPC decreases from 0.8Å.cy^{-1} to 0.5Å.cy^{-1} and high-temperature range (250-350 °C) in which GPC increases from 0.6Å.cy^{-1} to 0.9Å.cy^{-1} . In the low-temperature range, GPC is mainly influenced by the concentration of OH-groups (or water molecules) on the TiO_2 surface, which decreases as the substrate temperature increases. In the high-temperature range, GPC is influenced by the decomposition of TDMAT precursor on the TiO_2 surface, which leads to more active surface sites for reaction with water molecules. We found that water purge takes time in the low-temperature range, this may explain the different final GPC values reported in the literature. In the high-temperature region, the GPC difference reported in the literature can be explained by the different TDMAT pulse time leading to different amounts of TDMAT molecules for the chemical reactions, since the decomposition of TDMAT strongly depends on the time of reaction at this temperature range. We demonstrated that the 14 nm TiO_2 layer grown at 200 °C is amorphous and can be crystallized to Anatase after annealing. We found that the initial stages of TiO_2 ALD depend

on the substrate surface, *i.e.* a substrate-enhanced growth on SiO_2/Si surface and substrate-inhibited growth on InGaAs surface.

6. Acknowledgements

E.V.S. was supported by ANR project ANR-18-CE09-0031-03 (ULTIMED project). Financial support by the ANR project ANR-18-CE09-0031-03 and by the Centre of Excellence of Multifunctional Architectured Materials (Labex CEMAM) ANR-10-LABX-44-01 is gratefully acknowledged. The Ph.D. work of P.A.Y. is financed by the Labex MINOS (ANR-10-LABX-55-01). We acknowledge D. De Barros for ALD reactor engineering assistance, and C. Jiménez for FTIR measurements support. The authors acknowledge the facilities and the scientific and technical assistance of the CMTC characterization platform of Grenoble INP supported by the Centre of Excellence of Multifunctional Architectured Materials "CEMAM" n°ANR-10-LABX-44-01 funded by the "Investments for the Future" Program. We thank C. Cheriyan for the language consulting.

References

[1] D. A. Hanaor, C. C. Sorrell, Review of the anatase to rutile phase transformation, Journal of Materials science 46 (4) (2011) 855–874. doi:https://doi.org/10.1007/s10853-010-5113-0.

[2] X. Chen, S. S. Mao, Titanium dioxide nanomaterials: synthesis, properties, modifications, and applications, Chemical reviews 107 (7) (2007) 2891–2959. doi:https://doi.org/10.1021/cr0500535.

[3] B. Pant, M. Park, S.-J. Park, Recent advances in tio2 films prepared by sol-gel methods for photocatalytic degradation of organic pollutants and antibacterial activities, Coatings 9 (10) (2019) 613. doi:https://doi.org/10.3390/coatings9100613.

[4] C. W. Dunnill, A. Kafizas, I. P. Parkin, Cvd production of doped titanium dioxide thin films, Chemical Vapor Deposition 18 (4-6) (2012) 89–101. doi:https://doi.org/10.1002/cvde.201200048.

[5] Y. Kuzminykh, A. Dabirian, M. Reinke, P. Hoffmann, High vacuum chemical vapour deposition of oxides:: A review of technique development and precursor selection, Surface and Coatings Technology 230 (2013) 13–21. doi:https://doi.org/10.1016/j.surfcoat.2013.06.059.

[6] Y.-H. Wang, K. H. Rahman, C.-C. Wu, K.-C. Chen, A review on the pathways of the improved structural characteristics and photocatalytic performance of titanium dioxide (tio2) thin films fabricated by the magnetron-sputtering technique, Catalysts 10 (6) (2020) 598. doi:https://doi.org/10.3390/catal10060598.

[7] H. M. Ali, H. Babar, T. R. Shah, M. U. Sajid, M. A. Qasim, S. Javed, Preparation techniques of tio2 nanofluids and challenges: a review, Applied Sciences 8 (4) (2018) 587. doi:https://doi.org/10.3390/app8040587.

[8] V. Miikkulainen, M. Leskelä, M. Ritala, R. L. Puurunen, Crystallinity of inorganic films grown by atomic layer deposition: Overview and general trends, Journal of Applied Physics 113 (2) (2013) 2. doi:https://doi.org/10.1063/1.4757907.

[9] S. M. George, Atomic layer deposition: an overview, Chemical reviews 110 (1) (2010) 111–131. doi:https://doi.org/10.1021/cr900056b.

[10] J.-P. Niemelä, G. Marin, M. Karppinen, Titanium dioxide thin films by atomic layer deposition: a review, Semiconductor Science and Technology 32 (9) (2017) 093005. doi:https://doi.org/10.1088/1361-6641/aa78ce.

[11] M. Ritala, M. Leskelä, E. Nykänen, P. Soininen, L. Niinistö, Growth of titanium dioxide thin films by atomic layer epitaxy, Thin Solid Films 225 (1-

2) (1993) 288–295. doi:https://doi.org/10.1016/0040-6090(93)90172-L.

[12] G. T. Lim, D.-H. Kim, Characteristics of tiox films prepared by chemical vapor deposition using tetrakis-dimethyl-amido-titanium and water, Thin Solid Films 498 (1-2) (2006) 254–258. doi:https://doi.org/10.1016/j.tsf.2005.07.121.

[13] W. Maeng, H. Kim, Thermal and plasma-enhanced ald of ta and ti oxide thin films from alkylamide precursors, Electrochemical and Solid State Letters 9 (6) (2006) G191. doi:https://doi.org/10.1149/1.2186427.

[14] Q. Xie, Y.-L. Jiang, C. Detavernier, D. Deduytsche, R. L. Van Meirhaeghe, G.-P. Ru, B.-Z. Li, X.-P. Qu, Atomic layer deposition of ti o 2 from tetrakis-dimethyl-amido titanium or ti isopropoxide precursors and h 2 o, Journal of applied physics 102 (8) (2007) 083521. doi:https://doi.org/10.1063/1.2798384.

[15] J. Dendooven, S. Pulinthanathu Sree, K. De Keyser, D. Deduytsche, J. A. Martens, K. F. Ludwig, C. Detavernier, In situ x-ray fluorescence measurements during atomic layer deposition: Nucleation and growth of tio2 on planar substrates and in nanoporous films, The Journal of Physical Chemistry C 115 (14) (2011) 6605–6610. doi:https://doi.org/10.1021/jp111314b.

[16] H. Kang, C.-S. Lee, D.-Y. Kim, J. Kim, W. Choi, H. Kim, Photocatalytic effect of thermal atomic layer deposition of tio2 on stainless steel, Applied Catalysis B: Environmental 104 (1-2) (2011) 6–11. doi:https://doi.org/10.1016/j.apcatb.2011.03.010.

[17] S. Pulinthanathu Sree, J. Dendooven, J. Jammaer, K. Masschaele, D. Deduytsche, J. DHaen, C. E. Kirschhock, J. A. Martens, C. Detavernier, Anisotropic atomic layer deposition profiles of tio2 in hierarchical silica material with multiple porosity, Chemistry of Materials 24 (14) (2012) 2775–2780. doi:https://doi.org/10.1021/cm301205p.

[18] H. Tiznado, D. Dominguez, W. d. l. Cruz, R. Machorro, M. Curiel, G. Soto, Tio2 and al2o3 ultra thin nanolaminates growth by ald; instrument automation and films characterization, Revista mexicana de física 58 (6) (2012) 459–465.

[19] B. Abendroth, T. Moebus, S. Rentrop, R. Strohmeyer, M. Vinnichenko, T. Weling, H. Stöcker, D. C. Meyer, Atomic layer deposition of tio2 from tetrakis (dimethylamino) titanium and h2o, Thin Solid Films 545 (2013) 176–182. doi:https://doi.org/10.1016/j.tsf.2013.07.076.

[20] A. G. Scheuermann, J. P. Lawrence, M. Gunji, C. E. Chidsey, P. C. McIntyre, Ald-tio2 preparation and characterization for metal-insulator-silicon photoelectrochemical applications, ECS Transactions 58 (10) (2013) 75. doi:https://doi.org/10.1149/05810.0075ecst.

[21] M. Reiners, K. Xu, N. Aslam, A. Devi, R. Waser, S. Hoffmann-Eifert, Growth and crystallization of tio2 thin films by atomic layer deposition using a novel amido guanidinate titanium source and tetrakis-dimethylamido-titanium, Chemistry of Materials 25 (15) (2013) 2934–2943. doi:https://doi.org/10.1021/cm303703r.

[22] S. Rentrop, T. Moebus, B. Abendroth, R. Strohmeyer, A. Schmid, T. Weling, J. Hanzig, F. Hanzig, H. Stöcker, D. Meyer, Atomic layer deposition of strontium titanate films from sr (ipr3cp) 2, ti [n (ch3) 2] 4 and h2o, Thin solid films 550 (2014) 53–58. doi:https://doi.org/10.1016/j.tsf.2013.10.043.

[23] A. P. Didden, J. Middelkoop, W. F. Besling, D. E. Nanu, R. van de Krol, Fluidized-bed atomic layer deposition reactor for the synthesis of core-shell nanoparticles, Review of Scientific Instruments 85 (1) (2014) 013905. doi:https://doi.org/10.1063/1.4863099.

[24] S. Cao, J. Wang, H. Wang, Atomic layer deposited titanium dioxide coatings on kd-ii silicon carbide fibers and their characterization, Applied

Surface Science 367 (2016) 190–196. doi:https://doi.org/10.1016/j.apsusc.2016.01.183.

[25] A. Chaker, P. Szkutnik, J. Pointet, P. Gonon, C. Vallée, A. Bsiesy, Understanding the mechanisms of interfacial reactions during tio2 layer growth on ruo2 by atomic layer deposition with o2 plasma or h2o as oxygen source, Journal of Applied Physics 120 (8) (2016) 085315. doi:https://doi.org/10.1063/1.4960139.

[26] A. Haider, M. Yilmaz, P. Deminskyi, H. Eren, N. Biyikli, Nanoscale selective area atomic layer deposition of tio 2 using e-beam patterned polymers, RSC advances 6 (108) (2016) 106109–106119. doi:https://doi.org/10.1039/C6RA23923D.

[27] A. R. Head, S. Chaudhary, G. Olivieri, F. Bournel, J. N. Andersen, F. Rochet, J.-J. Gallet, J. Schnadt, Near ambient pressure x-ray photoelectron spectroscopy study of the atomic layer deposition of tio2 on ruo2 (110), The Journal of Physical Chemistry C 120 (1) (2016) 243–251. doi:https://doi.org/10.1021/acs.jpcc.5b08699.

[28] H. Borbón-Nuñez, D. Dominguez, F. Muñoz-Muñoz, J. Lopez, J. Romo-Herrera, G. Soto, H. Tiznado, Fabrication of hollow tio2 nanotubes through atomic layer deposition and mwcnt templates, Powder Technology 308 (2017) 249–257. doi:https://doi.org/10.1016/j.powtec.2016.12.001.

[29] L. Ye, J. A. Kropp, T. Gougousi, In situ infrared spectroscopy study of the surface reactions during the atomic layer deposition of tio2 on gaas (100) surfaces, Applied Surface Science 422 (2017) 666–674. doi:https://doi.org/10.1016/j.apsusc.2017.05.264.

[30] S. Zhuiykov, M. K. Akbari, Z. Hai, C. Xue, H. Xu, L. Hyde, Wafer-scale fabrication of conformal atomic-layered tio2 by atomic layer deposition using tetrakis (dimethylamino) titanium and h2o precursors, Materials & Design

120 (2017) 99–108. doi:https://doi.org/10.1016/j.matdes.2017.02.016.

[31] P. Birnal, M. M. de Lucas, I. Pochard, B. Domenichini, L. Imhoff, Photocatalytic properties of atomic layer deposited tio2 inverse opals and planar films for the degradation of dyes, Applied Surface Science 512 (2020) 145693. doi:https://doi.org/10.1016/j.apsusc.2020.145693.

[32] M. E. Dufond, M. W. Diouf, C. Badie, C. Laffon, P. Parent, D. Ferry, D. Grosso, J. C. Kools, S. D. Elliott, L. Santinacci, Quantifying the extent of ligand incorporation and the effect on properties of tio2 thin films grown by atomic layer deposition using an alkoxide or an alkylamide, Chemistry of Materials 32 (4) (2020) 1393–1407. doi:https://doi.org/10.1021/acs.chemmater.9b03621.

[33] S. S. Vandenbroucke, E. Levrau, M. M. Minjauw, M. Van Daele, E. Solano, R. Vos, J. Dendooven, C. Detavernier, Study of the surface species during thermal and plasma-enhanced atomic layer deposition of titanium oxide films using in situ ir-spectroscopy and in vacuo x-ray photoelectron spectroscopy, Physical Chemistry Chemical Physics 22 (17) (2020) 9262–9271. doi:https://doi.org/10.1039/D0CP00395F.

[34] E. V. Skopin, L. Rapenne, H. Roussel, J.-L. Deschanvres, E. Blanquet, G. Ciatto, D. D. Fong, M.-I. Richard, H. Renevier, The initial stages of zno atomic layer deposition on atomically flat in 0.53 ga 0.47 as substrates, Nanoscale 10 (24) (2018) 11585–11596. doi:https://doi.org/10.1039/C8NR02440E.

[35] E. Skopin, L. Rapenne, J. Deschanvres, E. Blanquet, G. Ciatto, L. Pithan, D. Fong, M.-I. Richard, H. Renevier, In situ x-ray studies of the incipient zno atomic layer deposition on in 0.53 ga 0.47 as, Physical Review Materials 4 (4) (2020) 043403. doi:https://doi.org/10.1103/PhysRevMaterials.4.043403.

[36] E. V. Skopin, J.-L. Deschanvres, H. Renevier, In situ ellipsometry study of the early stage of zno atomic layer deposition on in0. 53ga0. 47as, physica status solidi (a) 217 (8) (2020) 1900831. doi:https://doi.org/10.1002/pssa.201900831.

[37] M.-H. Chu, L. Tian, A. Chaker, E. Skopin, V. Cantelli, T. Ouled, R. Boichot, A. Crisci, S. Lay, M.-I. Richard, et al., Evaluation of alternative atomistic models for the incipient growth of zno by atomic layer deposition, Journal of Electronic Materials 46 (6) (2017) 3512–3517. doi:https://doi.org/10.1007/s11664-017-5448-2.

[38] Y. Sun, P. Pianetta, P.-T. Chen, M. Kobayashi, Y. Nishi, N. Goel, M. Garner, W. Tsai, Arsenic-dominated chemistry in the acid cleaning of ingaas and inalas surfaces, Applied Physics Letters 93 (19) (2008) 194103. doi:https://doi.org/10.1063/1.3025852.

[39] Filmsence llc, fs-1 manual, http://www.film-sense.com/.

[40] R. Boichot, L. Tian, M.-I. Richard, A. Crisci, A. Chaker, V. Cantelli, S. Coindeau, S. Lay, T. Ouled, C. Guichet, et al., Evolution of crystal structure during the initial stages of zno atomic layer deposition, Chemistry of Materials 28 (2) (2016) 592–600. doi:https://doi.org/10.1021/acs.chemmater.5b04223.

[41] M. H. Chu, L. Tian, A. Chaker, V. Cantelli, T. Ouled, R. Boichot, A. Crisci, S. Lay, M.-I. Richard, O. Thomas, et al., An atomistic view of the incipient growth of zinc oxide nanolayers, Crystal Growth & Design 16 (9) (2016) 5339–5348. doi:https://doi.org/10.1021/acs.cgd.6b00844.

[42] B. A. Sperling, J. Hoang, W. A. Kimes, J. E. Maslar, K. L. Steffens, N. V. Nguyen, Time-resolved surface infrared spectroscopy during atomic layer deposition of tio2 using tetrakis (dimethylamido) titanium and water, Journal of Vacuum Science & Technology A: Vacuum, Surfaces, and Films 32 (3) (2014) 031513. doi:https://doi.org/10.1116/1.4872166.

[43] J. P. Driessen, J. Schoonman, K. F. Jensen, Infrared spectroscopic study of decomposition of ti (n (ch 3) 2) 4, Journal of The Electrochemical Society 148 (3) (2001) G178–G184. doi:https://doi.org/10.1149/1.1350687.

[44] L. E. Walle, A. Borg, E. Johansson, S. Plogmaker, H. Rensmo, P. Uvdal, A. Sandell, Mixed dissociative and molecular water adsorption on anatase tio2 (101), The Journal of Physical Chemistry C 115 (19) (2011) 9545–9550. doi:https://doi.org/10.1021/jp111335w.

[45] P. Karlsson, J. Richter, M. P. Andersson, M.-J. Johansson, J. Blomquist, P. Uvdal, A. Sandell, Tio2 chemical vapor deposition on si (111) in ultrahigh vacuum: Transition from interfacial phase to crystalline phase in the reaction limited regime, Surface Science 605 (13-14) (2011) 1147–1156. doi:https://doi.org/10.1016/j.susc.2011.03.001.

[46] A. R. Head, N. Johansson, Y. Niu, O. Snezhkova, S. Chaudhary, J. Schnadt, H. Bluhm, C. Chen, J. Avila, M.-C. Asensio, In situ characterization of the deposition of anatase tio2 on rutile tio2 (110), Journal of Vacuum Science & Technology A: Vacuum, Surfaces, and Films 36 (2) (2018) 02D405. doi:https://doi.org/10.1116/1.5005533.

[47] R. Gonzalez, R. Zallen, H. Berger, Infrared reflectivity and lattice fundamentals in anatase tio 2 s, Physical Review B 55 (11) (1997) 7014. doi:https://doi.org/10.1103/PhysRevB.55.7014.

[48] R. L. Puurunen, W. Vandervorst, Island growth as a growth mode in atomic layer deposition: A phenomenological model, Journal of Applied Physics 96 (12) (2004) 7686–7695. doi:https://doi.org/10.1063/1.1810193.

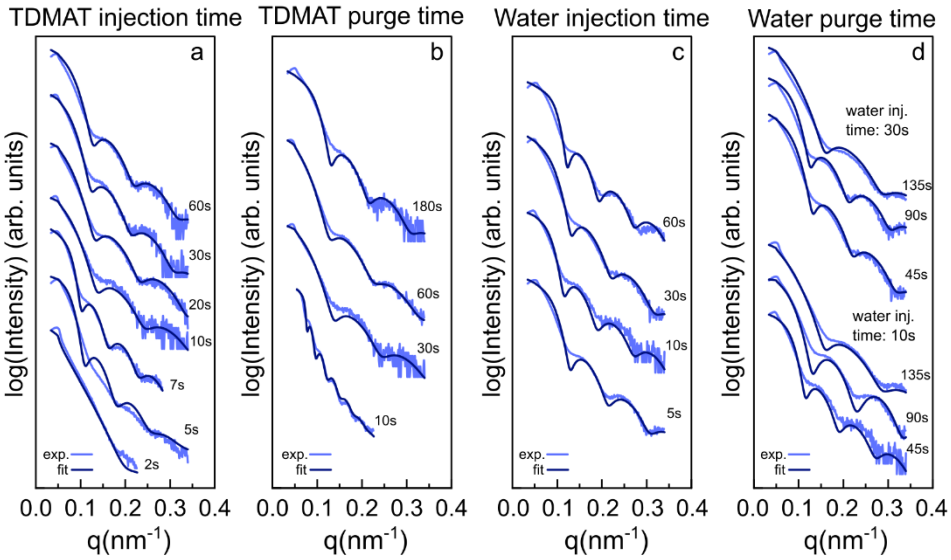

Figure S1. X-Ray Reflectivity (XRR) curves, measured after the growth of TiO_2/Si samples. The different purge/pulse parameters were varied: (a) TDMAT pulse time was 2, 5, 7, 10, 20, 30, 60s; (b) TDMAT purge time was 10, 30, 60, 180s; (c) Water pulse time was 5, 10, 30, 60s; and (d) Water purge time was 45, 90, 130s for fixed water pulse time at 10s and 30s.

Table T1. The thickness of TiO_2 layers obtained after experimental x-ray reflectivity curves fit.

Parameter		Time (s)	Number of cycles	TiO_2 thickness (nm)
TDMAT injection time		60	50	9.7±0.5
		30	50	10.3±0.3
		20	50	9.1±0.6
		10	50	8.6±1.1
		7	120	13.7±0.6
		5	150	12.0±1.6
		2	185	5.4±1.1
TDMAT purge time		180	60	10.1±0.4
		60	60	9.2±1.2
		30	50	8.6±1.1
		10	200	29.9±5.5
Water injection time		60	100	11.6±0.4
		30	100	9.8±0.3
		10	130	11.5±0.8
		5	140	10.1±0.7
Water purge time	10s of water injection	135	125	7.2±0.2
		90	150	9.2±0.1
		45	130	11.5±0.8
	30s of water injection	135	130	8.0±0.3
		90	140	10.2±0.3
		45	100	9.8±0.3

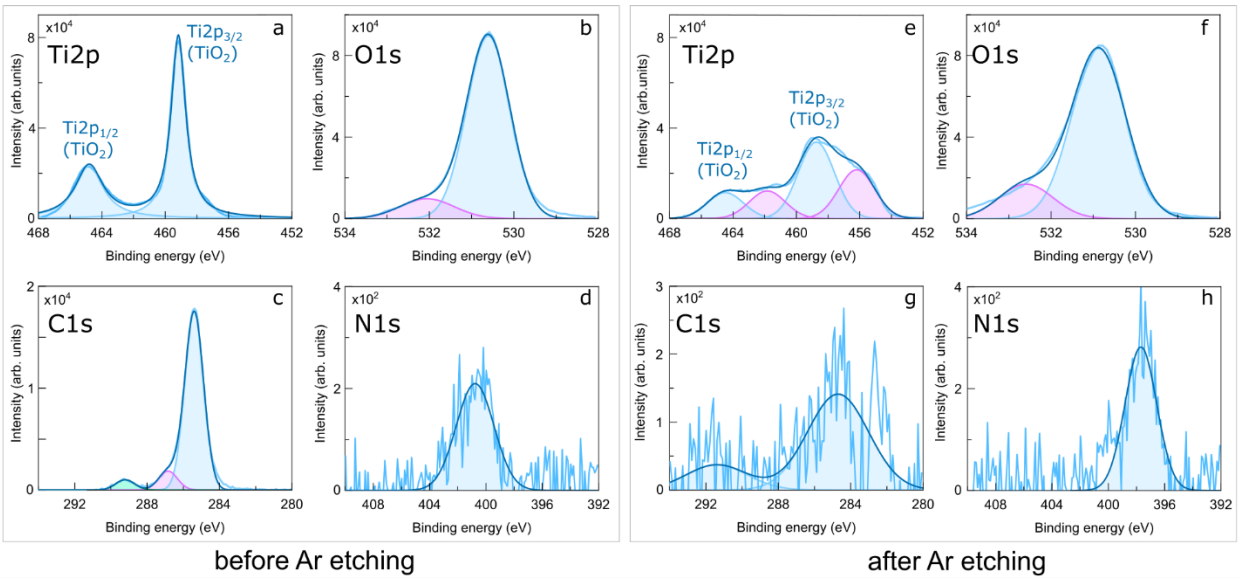

Figure S2. X-ray photoelectron spectroscopy (XPS) lines of a 14nm thick amorphous TiO_2 layer measured before (a-d) and after (e-h) Ar plasma etching: (a,e) Ti2p, (b,f) O1s, (c,g) C1s, (d,h) N1s.

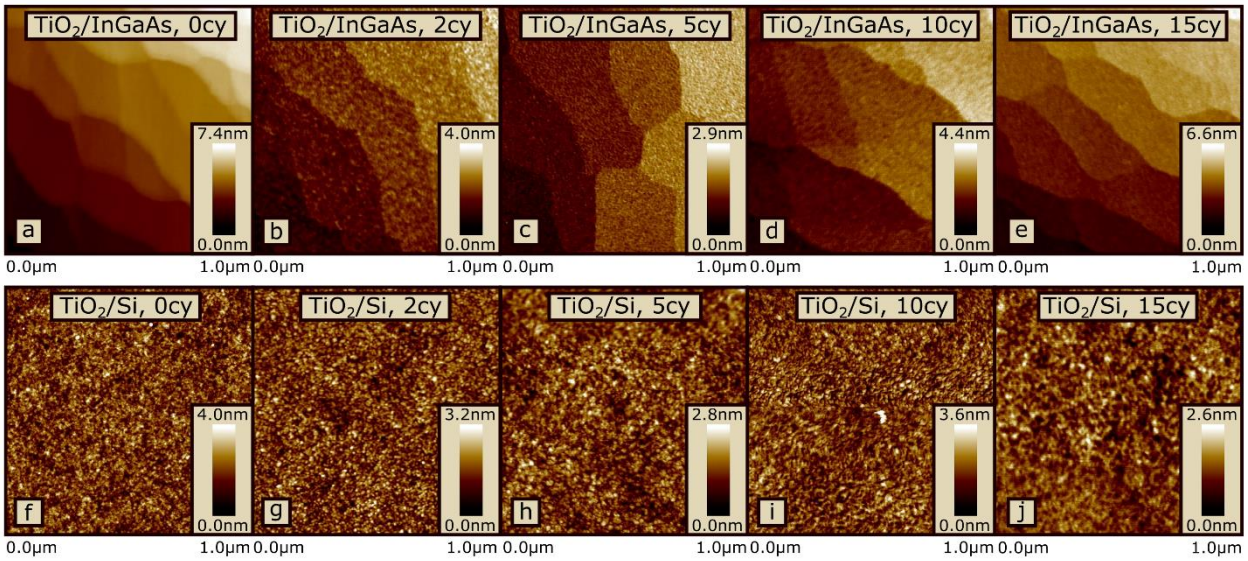

Figure S3. (1x1)µm^2 AFM images measured for (a-e) TiO_2/ InGaAs and (f-j) TiO_2/ Si series of samples with a different number of ALD cycles: (a,f) 0cy or substrate, (b,g) 2cy, (c,h) 5cy, (d,i) 10cy, and (e,j) 15cy.